Journal of Soils and Sediments
https://doi.org/10.1007/s11368-019-02355-x

SEDIMENTS, SEC 2 • PHYSICAL AND BIOGEOCHEMICAL PROCESSES • RESEARCH ARTICLE

Microscale distribution of trace elements: a methodology for accessing major bearing phases in stream sediments as applied to the Loire basin (France)

Cecile Grosbois[1] · Alexandra Courtin-Nomade[2]

Received: 21 November 2018 / Accepted: 19 May 2019

Abstract

Purpose The threat of trace elements (TE) stored in sediments depends on total concentrations, their chemical form, and also on the type of TE–particle association and their resultant stability. The present study aimed at identifying the major TE-bearing phases in river sediments and quantifying their in situ concentrations once total concentrations of TE had been determined in order to understand potential TE mobility and ensuing environmental risk during early diagenesis mechanisms and the sediment cascade.

Materials and methods Several TE-enriched layers of sediment cores were selected in a polymetallic-contaminated river basin (Loire basin, France). Selected samples were taken from up- and downstream areas far from sites of specific mining, or heavy industrial or urban activities. They thus represent non-site-dependent sediments which were not modulated or controlled by specific mineralogy or anthropogenic activities. Detailed microscale investigation techniques (SEM, EPMA, and μSXRD) were used to characterize directly the complex TE–solid phase association within river sediments. Despite Bi, Cd, and Hg representing the highest enrichment of the studied sediment layers, these elements were not detected at a microscale and only ubiquitous TE such as As, Cu, Pb, and Zn could be quantified on polished thin sections (EPMA quantification limit = 1000 mg kg^{-1}, $n = 111$).

Results and discussion Three mineralogical groups were evidenced by PCA, EPMA, and μSXRD data. (i) Fine-grained aggregates of aluminosilicates were frequently detected, appearing multiphased in organic matrices. They were mostly enriched with Zn and Pb without any As or Cu. (ii) (Mn, Ti)-rich Fe oxyhydroxides were predominantly SEM observed, either as isolated grains, silicate coatings, or included in aggregates. They represented the highest detected in situ concentrations for all the studied TE. And finally, (iii) Mn-rich particles were not frequently observed with SEM but when present were characterized by the highest TE concentrations. Phosphates, carbonates, and S-rich particles (sulfides and/or sulfates) were also determined by PCA as a potential mineralogical group. However, due to their very low TE concentrations and frequency, they could not be considered representative of a TE-bearing mineralogical group.

Conclusions This fine sorting classification, combining different techniques at the particle scale, was used to visualize and quantify complex mineralogy and particle associations of TE-bearing phases in river bed sediments under no specific mineralogical control. It represents an interesting approach to understand TE mobility during sediment cascade and post-depositional processes in sediments.

Keywords Bearing phases · Loire basin · Secondary minerals · Sediments · Trace elements · Trace element mobility

Responsible editor: Patrick Byrne

Electronic supplementary material The online version of this article (https://doi.org/10.1007/s11368-019-02355-x) contains supplementary material, which is available to authorized users.

✉ Cecile Grosbois
cecile.grosbois@univ-tours.fr

[1] Université de Tours EA 6293 GéoHydrosystèmes continentaux, Parc de Grandmont, 37200 Tours, France

[2] Université de Limoges EA 7500 PEIRENE, 123 avenue Albert Thomas, 87060 Limoges, France

1 Introduction

Over recent decades, many trace elements (TE) have been identified as major harmful elements with significant ecological and health issues in various environments of the critical zone such as surface and groundwaters, sediments, and soil horizons (Dudka and Adriano 1997; Forstner and Salomons 2008; Kabata-Pendias and Sadurski 2008; Nriagu and Skaar 2015; Bonner and Bridges 2016). Many studies have successfully characterized the spatial distribution of trace element concentrations at a basin scale (e.g., Garban et al. 1996;

Published online: 18 June 2019

Forstner et al. 2004; Horowitz and Stephen 2008; Frau et al. 2009; Larrose et al. 2010; Bednarova et al. 2013; Garcia-Lorenzo et al. 2014) and the temporal dynamics in soils and river sediments (Audry et al. 2004; Le Cloarec et al. 2009; Zhou et al. 2014; Dhivert et al. 2016) and have also differentiated detrital from anthropogenic sources (Novakova et al. 2013; Miler and Gosar 2015).

The chemical properties of TE result in them being concentrated mainly in the solid fraction (Horowitz and Elrick 1987) and enable a variety of bonds to be formed with particles (Charlet and Manceau 1993; Sparks 2005; Du Laing et al. 2009). Trace elements can be sorbed or included in the crystal lattice, in anthropogenic alloys, airborne particles, primary or secondary minerals, or organic matter complexes.

According to variations in river conditions (changes of pH, ionic strength, oxic and anoxic conditions, and/or microbial communities) which influence the stability of TE–particle bonds, the fate of TE can vary greatly in rivers. Trace elements can be (i) kept in a crystal lattice (detrital primary phases) and transported downstream with sediment particles, (ii) released slowly into surface waters when bearing phases are altered during sediment transport, (iii) released easily into interstitial waters in naturally occurring suboxic–anoxic transition zones due to the dissolution of host phases, and (iv) trapped post-deposition during early diagenetic processes and the formation of secondary phases (i.e., sulfides, hydroxides). Hence, TE cycling is highly dependent on the resultant stability of bearing phases under sediment transport conditions. The threat of trace elements stored in sediments depends on total concentrations, geochemical behavior of the TE, and also on the type of TE–particle association and stability.

Four main types of TE-bearing phases are commonly described in the literature: (Fe, Mn) oxyhydroxides, clay minerals, sulfides, and organic matter. They are usually characterized by geochemical models (Ryan et al. 2008; Blute et al. 2009; Drahota et al. 2009; Potsma et al. 2010) and/or sequential and selective extraction protocols (e.g., Ciffroy et al. 2003; Frau et al. 2009; Favas et al. 2011) in order to quantify the percentage of TE associated with each type. Specifying TE through sequential extraction provides an overview of the behavior of the elements according to geochemical changes in the environment such as pH or Eh variations. Although numerous protocols exist, they are not necessarily selective and in particular, clay minerals can change and secondary minerals can be formed during extraction procedures (Gleyzes et al. 2002; Hudson-Edwards et al. 2004; Ryan et al. 2008; Villanueva et al. 2013; Jack et al. 2015). Few studies have determined TE-bearing mineralogy in sediments at a microscopic scale (Drahota et al. 2009; Frau et al. 2009; Grosbois et al. 2011; Montarges-Pelletier et al. 2014; Byrne et al. 2017; Costa-Miguens et al. 2016). However, regarding environmental studies, policymakers, and stakeholder management reports, it is important to be able to assess potential TE sources and their fate over time for future sediment management. Mineralogical characterization should become a mandatory step to link TE-bearing mineral stability to future TE release into the water column. In fact, elemental composition does not provide information concerning the reactivity or behavior of a mineral but by using mineralogical characterization, it is possible to identify how an element is bound to an organic or inorganic phase. This thus provides information about its stability regarding the chemical bond involved, the conditions of formation, and the geochemical parameters required for this phase to be stable.

In this context, the present study addressed different and ubiquitous TE in sediments. The main purpose was to identify TE-bearing phases at a particle observation scale in order to assess TE mobility during early diagenesis mechanisms and sediment transport once total concentrations of TE had been quantified. This approach was applied at a basin scale in Loire river sediments (France). This basin presents some specific geochemical anomalies and lithology (Carroué 2010; Macaire et al. 2013). The sediment layers selected were TE enriched but were located far from any areas of specific mining, heavy industrial, or urban activities (Grosbois et al. 2012; Dhivert et al. 2016).

2 Materials and methods

2.1 Study area and materials

The Loire river basin is the largest drainage basin in France (1013 km long with a drainage surface of 117,800 km^2), presenting contrasting geology and hydrology between up- and downstream sections. Over the last decade, studies investigating the quality of Loire river sediments regarding TE on multisite sedimentary cores throughout the basin have highlighted the high levels of contamination compared with other French river basins (Grosbois et al. 2012). Different contamination periods have also been well-documented (Dhivert et al. 2016). Firstly, an important but local Sb contamination was evidenced in the upper Loire basin between the early 1900s and the 1950s, related to local Sb mining and associated activities. A second general polymetallic contamination phase occurred at the basin scale, in the upper part between the 1940s and 1950s, and the most downstream part of the basin between the 1950s and 1980s. Since the 1980s, a global decline in trace metal concentrations can be observed related to de-industrialization, mine and industry closure, and improvements in wastewater treatment (Grosbois et al. 2012; Dhivert et al. 2016). In addition, it is necessary to take into account the sediment cascade in this basin, as well as the hydro-sedimentary dynamic which is also an important factor in the reactivation of old and temporary trace-element sources during major flood events as shown by Dhivert et al. (2015). These mechanisms have been reported in other basins (Le Gall et al. 2017).

The material studied came from two sediment cores taken from up- and downstream sites of the Loire river basin: the upstream station at Villerest dam (KP 741–6516 km^2, about 40% of the total drainage basin) and the downstream station situated immediately upstream of the estuary entrance at Montjean (KP 0–109,930 km^2; Fig. 1). The location of these two stations can be considered as representative of the lithology drained by the whole Loire river basin. The upstream core station mostly drains Paleozoic/Variscan granites, gneiss, and micaschists (500–300 Ma), covered by sedimentary bedrock of Carboniferous sandstones and Oligocene–Miocene fluviolacustrine deposits, sandstones, marls, and clays (infoterre.brgm.fr, 2017). The downstream station includes the geology drained from this upstream section, and also marine and continental sedimentary bedrock of the Parisian basin including ~ 30% of limestones, chalk, and marl layers; ~ 24% of detrital siliceous rocks; and less than 5% of present-day alluvial deposits (BRGM 2017).

The two sampling stations studied were also far enough from any geochemical anomaly or associated specific mineralogy such as barite, fluorite, or sulfides (Carroué 2010). The stations were specifically chosen to be far from any potential input of heavy minerals (density > 2.89 such as kyanites, garnets, sphenes Macaire et al. 2013). According to petrographic analysis of Loire sediments by Macaire et al. (2013), sandy sediments stored in channels and floodplains of the Loire river are mainly composed of quartz, potassic feldspars, and plagioclases as well as plutonic, metamorphic, and volcanic bedrock fragments. These sediments are relatively immature compared with other fluvial basins under similar climatic conditions. Furthermore, the upstream crystalline part of the Loire basin is a larger contributor to sediments than the sedimentary area, particularly because of sedimentary reworking and anthropogenic activities (dam building and sand mining). According to X-ray diffraction analyses conducted on the bulk fraction of the sediment core levels studied and on the clay fraction (Electronic Supplementary Material, SI 1), sediments are mostly composed of quartz, K-feldspars (orthoclase-type), micas, clays, and clay minerals such as kaolinite, chlorite, and illite, in line with the clay mineral

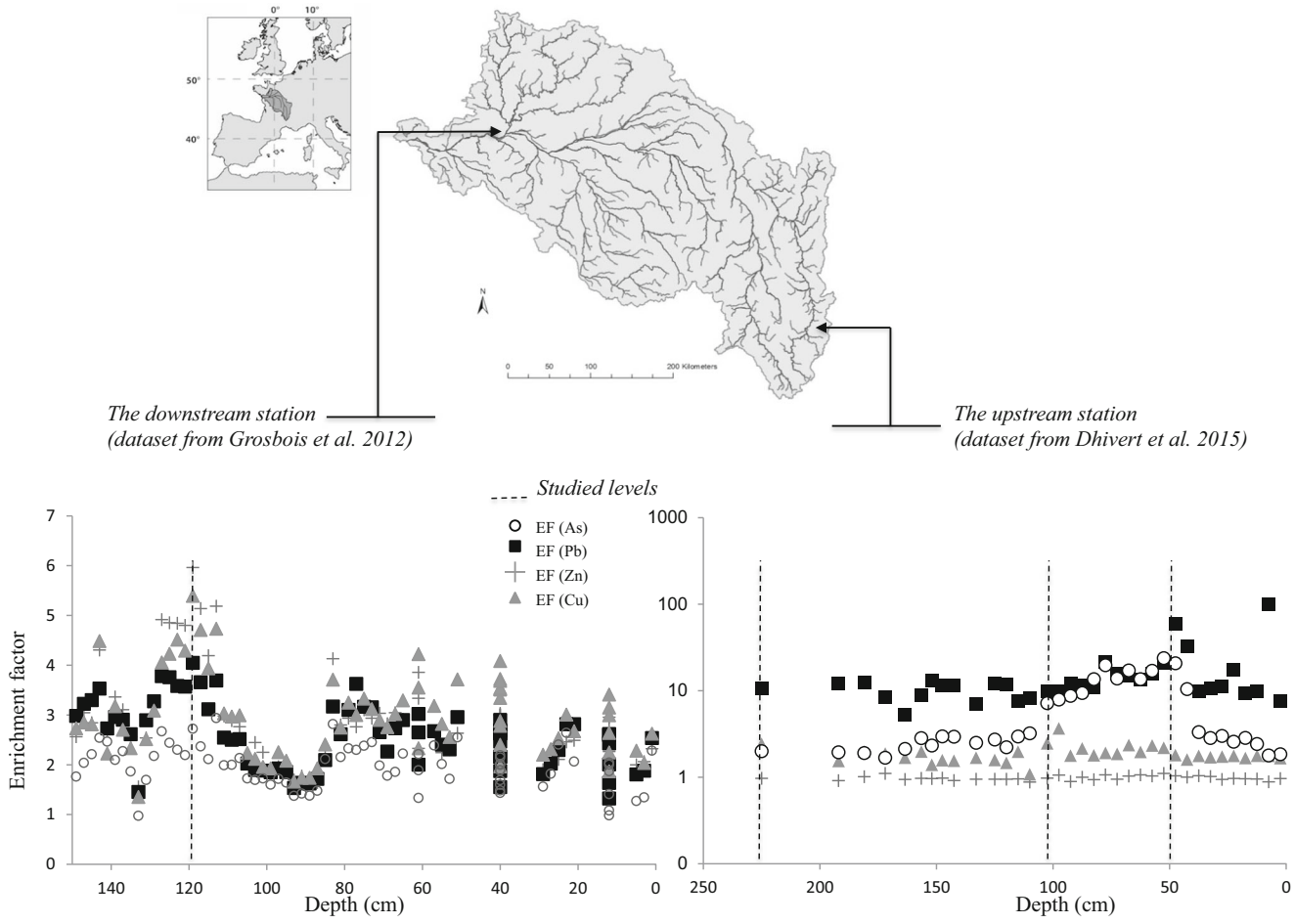

Fig. 1 Variations according to depth of sediment enrichment factors for As, Cu, Pb, and Zn at both stations of the Loire river basin (location marked on the associated maps). Enrichment factors were calculated in the < 63-μm fraction with a double normalization to Al concentrations and to the local geochemical background (Grosbois et al. 2012). Sediment layers for in situ characterization in this study are identified with dashed lines

assemblage of the whole basin as indicated by Brossé (1979, 1982) and Manickam et al. (1985). The most downstream station is more clayey and contains chlorite, illite, kaolinite, and micas. The upstream station contains no chlorite but only illite and micas (some kaolinite at the deepest levels; Electronic Supplementary Material, SI 1).

For the two sediment cores, the age models were based on ^{137}Cs activity peaks and variations in several sedimentary parameters (grain size, water content, Si/Al ratios, detrital element concentrations, and flood occurrence; Grosbois et al. 2012; Dhivert et al. 2015). Sediment accumulation at the upstream station was from the 1980s to 2012 and at the downstream station from < 1900 to 2009, which correspond to the sampling dates.

2.2 Bulk chemical composition of the materials studied

Shortly after sampling, sediments from the middle of the core liner were sampled every 2 cm with a ceramic knife in the laboratory. Each slice was then air-dried on a dark clean shelf for 1 day and sieved through 63-μm disposable Nylon mesh. Bulk concentrations were obtained on the < 63-μm fraction. Analytical procedures for the bulk chemical composition were described in detail in previous studies on sediment quality in Grosbois et al. (2012) and Dhivert et al. (2015, 2016).

Major element profiles have been presented in previous articles. Briefly, the three most concentrated major elements at both stations were Si > Al > Fe, K (Table 1). Silicon, Al, and K were quite stable throughout both cores linked to the aluminosilicate mineralogical assemblage, except when sand-rich detrital material was deposited during major flood events (Dhivert et al. 2015). The organic concentrations were low for these sediments with total organic carbon < 2.0%, and ranging between 1.7 and 3.6% for the upstream and downstream cores respectively (Grosbois et al. 2012; Dhivert et al. 2015). The major difference between the two cores studied was for Ca and total carbon compositions. At the downstream station, there was considerable Ca enrichment associated with a high particulate inorganic carbon content and several well-marked Ca peaks (Grosbois et al. 2012). In the middle basin, marked eutrophication started in the 1950s due to an increase in nutrients and precipitation of endogenic calcite was observed at different stations of the Middle and Lower Loire basin during low-flow periods (Manickam et al. 1985; Négrel 1997; Grosbois et al. 2001). No calcite precipitation was detected at the upstream station studied.

The sediment layers for this study at both stations were chosen according to the enrichment factor (EF), calculated as a double normalization to Al concentrations and to the local geochemical background in the < 63-μm fraction (analyzed at the downstream station in Montjean; Grosbois et al. 2012). These layers were either non-impacted sediment layers or

Table 1 Bulk concentrations of selected major and trace elements in < 63-μm sediment cores (minimum, maximum and at the studied depths) located at both up- and downstream stations of the Loire river basin and in the local geochemical background for comparison

	Si %wt	Al %wt	Fe %wt	Ti %wt	Mg %wt	Ca %wt	Na %wt	K %wt	TC %wt	As mg kg^{-1}	Cr mg kg^{-1}	Cu mg kg^{-1}	Ni mg kg^{-1}	Pb mg kg^{-1}	Zn mg kg^{-1}
Sediments at the most upstream studied station															
Minimum of the sediment core	21.4	7.8	3.2	0.45	0.91	0.58	0.42	2.05	3.0	22	96	30	38	49	146
Maximum of the sediment core	28.3	10.1	5.5	0.73	1.44	1.11	1.30	3.14	6.7	57	397	113	167	148	588
In the studied level (118–120 cm deep)	22.7	8.9	4.8	0.56	1.26	0.90	0.75	2.56	5.8	56	328	113	156	148	588
Sediments at the most downstream studied station															
Minimum of the sediment core	19.4	6.4	3.4	0.43	0.71	1.29	0.50	1.49	n.a.	1	103	20	n.a.	13	503
Maximum of the sediment core	26.9	8.6	5.1	0.71	1.06	9.79	1.03	2.42	n.a.	13	280	71	n.a.	213	693
In the studied level (50–55 cm deep)	20.6	7.0	3.7	0.49	0.78	7.88	0.58	1.78	11.8	13	280	35	n.a.	43	604
In the studied level (100–105 cm deep)	23.3	7.6	4.5	0.52	0.85	3.35	0.60	1.94	9.2	4	164	43	n.a.	22	581
In the studied level (220–230 cm deep)	24.6	8.5	5.1	0.71	1.06	1.52	0.81	2.28	6.7	1	130	48	n.a.	26	641
Local geochemical background in the Loire river basin (Grosbois et al. 2012; Dhivert et al. 2016)															
	26.4	8.5	4.3	0.75	0.94	1.57	0.96	2.35	n.a.	20	99	20	28	35	94

n.a. non-available

the most TE enriched, depending on the TE considered (Fig. 1). In each core studied, the highest enrichment factors were detected for Bi, Cd, and Hg, with EF values above 6 at the upstream station (Dhivert et al. 2015, 2016) and above 10 at the downstream station (Grosbois et al. 2012). High enrichment factors (EF > 3) were also observed for some frequent and ubiquitous TE, for example, As, Cu, Pb, and Zn. All the EF showed the same temporal variations along the sediment cores, but the intensities varied (Fig. 1). At the upstream station, the sediment level showing the highest EF was the 118–120-cm level (< 1980s). At this level, Zn was the most enriched TE, followed by Cu > Pb > As. At the downstream station, three sediment levels were selected according to EF variations: 50–55 (early 1980s), 100–105 (early 1950s), and 220–230-cm levels (< 1900s). The most enriched TE in these selected layers were Pb > As > Cu as was the case throughout the whole sediment core. Throughout the Loire basin, Zn is the most enriched TE (Dhivert et al. 2016); however, it was not enriched at this most downstream station, where its concentrations were close to the background level.

2.3 In situ characterization methods

In situ characterization was carried out on sediments that had been air-dried and 63 μm sieved. Shortly after sampling, polished thin sections of embedded sediments were formed using epoxy resin. Sections were mounted on a carbon sample holder, coated with a carbon layer of about 10 Å for observation under a scanning electron microscope (SEM) and electron probe microanalysis (EPMA). SEM observations were conducted using a backscattered electron beam with a working distance of 10 mm, a probe current set at 10 nA and 20 kV with a counting time of 60 s per analysis. Under these conditions, TE could be detected at concentrations greater than 1000–1500 ppm depending on the element. EPMA analyses were performed on SEM-selected particles at 15 kV with a 4-nA beam current; under these conditions, the detection limit ranged between 800 and 1000 ppm according to the TE of interest (Fialin et al. 1999). For the sake of representativeness, three to six analyses were carried out on each particle when it was long enough (> 10 μm) and mineralogically homogeneous. When the area analyzed combined several particles, each particle was analyzed two to three times according to its size.

In situ mineralogical characterization was carried out on selected particles/aggregates which could not be defined by chemical composition alone (Fe-Mn oxyhydroxides) or whose aggregate mineralogy was too complex. Microscanning X-ray diffraction (μSXRD) was performed at the ALS beamline 12.3.2 (Lawrence Berkeley National Lab, Ca, US; Kunz et al. 2009) with an analytical procedure defined in Courtin-Nomade et al. (2010) on the same polished thin sections as those used for SEM and EPMA analyses after the carbon coating had been removed. Each analyzed area was first mapped for Fe using microscanning X-ray fluorescence (μSXRF) on the same beamline and using a similar configuration as that used for μSXRD analyses. MicroSXRD patterns were then collected using a monochromatic mode because of the small size of the analyzed particles. Thin sections were mounted onto an XYZ stage horizontally tilted at 6°, with an incident X-ray energy of 10 keV, a beam size of 2 μm (H) × 20 μm (V) (beam footprint size on the sample of 20 μm (H) × 20 μm (V) FWHM), and a DECTRIS Pilatus 1M CCD detector (1 Å~1 k pixels binned mode). Acquisition times for micro X-ray patterns varied from 30 to 300 s according to the nature of the phase analyzed and its crystallinity in order to obtain significant intensity for each peak. Acquisition time for microXRD mineralogical maps varied from 6 to 8 h per map, depending on the size of the surface analyzed. Results were extracted using XMAS software (Tamura et al. 2005) and NIST corundum powder calibration material.

3 Results and discussion

3.1 Chemical characterization of TE-bearing phases

A first step involved statistical analysis of all the EPMA data to define the main representative groups of TE-bearing phases and their respective chemical composition. The EPMA analyses presented were validated according to two criteria: totals had to be greater than 50% to be significant, and representative concentrations were set to be higher than the quantification limit for all the TE studied (1000 mg kg^{-1}; MEN/CAMPARIS platform, pers.com.). For these reasons, in situ Bi, Cd, and Hg concentrations could not be detected significantly in individual grains with selective EPMA procedures even though these TE represented the highest enrichment factors in the bulk sediment fractions. Only in situ concentrations of As, Cr, Cu, Pb, and Zn were quantified significantly. Among 245 SEM-detected particles, 56 particles were selected for quantitative EPMA analyses. Among the 226 EPMA analyses performed, 111 were validated for both up- and downstream stations (53 and 58, respectively; Table 2) according to the criteria selected initially (totals and in situ TE concentrations higher than quantification limits).

A principal component analysis (PCA) was performed with in situ concentrations of all the analyzed particles. In situ concentrations were not replaced by any low value when below the detection limit. The chemical compositions of all the particles were included as objects (rows) in the data matrix, while major and trace element concentrations were used as variables (columns). The PCA was first performed for all the data and then divided into two different subgroups according to the location of the core site (up- or downstream site).

Among all the particles analyzed, six principal components (PCs) with eigenvalues greater than 1 explained 67% of the

Table 2 In situ concentrations of selected major and trace elements (EPMA determined) for the different types of trace element–bearing phases

	Si+Al %wt	Fe %wt	Mn %wt	Ti %wt	P %wt	S %wt	Mg %wt	Ca %wt	Na %wt	K %wt	As mg kg^{-1}	Cr mg kg^{-1}	Cu mg kg^{-1}	Ni mg kg^{-1}	Pb mg kg^{-1}	Zn mg kg^{-1}
Aluminosilicates ($n = 19$)																
Minimum	24.5	0.1	< QL	< QL	< QL	< QL	< QL	< QL	0.1	0.1	< QL	< QL	(720)	< QL	(870)	(970)
Maximum	41.4	5.5	0.2	5.5	0.9	0.2	1.3	12.2	4.9	12.7	< QL	< QL	(870)	< QL	2610	3390
(Fe, Ti)-rich silicate aggregates ($n = 23$)																
Minimum	12.7	4.8	< QL	0.1	< QL	< QL	< QL	< QL	< QL	< QL	< QL	720	< QL	< QL	< QL	(850)
Maximum	33.2	30.3	1.2	3.0	6.1	2.5	7.4	14.0	0.9	4.2	(730)	1080	< QL	1100	1700	3810
Fe oxyhydroxides ($n = 18$)																
Minimum	0.1	36.5	< QL	< QL	< QL	< QL	< QL	< QL	< QL	< QL	(770)	< QL	(680)	< QL	(770)	< QL
Maximum	14.3	70.2	0.8	0.6	1.8	0.9	4.5	1.3	0.4	0.7	2040	1300	2000	1650	2540	16,910
Mn-rich Fe oxyhydroxides ($n = 24$)																
Minimum	0.2	19.2	1.0	< QL	0.2	< QL	< QL	< QL	0.1	0.1	< QL	< QL	< QL	< QL	(830)	< QL
Maximum	13.5	46.6	7.5	1.6	3.5	0.7	0.8	0.8	3.1	13.1	< QL	750	1210	(950)	1950	22,960
(Fe, Ti) oxides ($n = 19$)																
Minimum	0.5	32.7	0.3	2.3	< QL	< QL	0.6	< QL	< QL	< QL	< QL	< QL	1150	< QL	< QL	< QL
Maximum	8.1	62.9	0.9	14.8	1.8	0.1	3.1	1.0	0.8	0.2	< QL	2060	1390	1020	8180	4860
Mn-rich particles ($n = 8$)																
Minimum	6.6	2.1	21.2	< QL	0.2	< QL	< QL	0.2	0.1	0.2	< QL	< QL	< QL	(760)	1070	2590
Maximum	14.4	4.5	31.9	1.1	0.7	0.2	0.9	3.6	2.6	1.6	(740)	< QL	2570	7550	5190	16,840

< *QL* below quantification limit, *n* number of EPMA analyses; concentrations in brackets refer to significantly detected elements but below quantification limit

total variance (Table 3a). The first PC (PC1), accounting for 19.0%, showed positive contributions of Si, Al, and K concentrations and a negative contribution of Fe concentrations. Most PC1 elements were major lithophile elements associated with aluminosilicates contributing positively and Fe oxyhydroxides contributing negatively, but no TE was significantly representative in this component. The second PC (PC2), which accounted for 15.1% of the total variance, was associated with Mn, Cu, Ni, and Zn concentrations. Hence, Mn-rich particles were either Mn oxyhydroxides or Mn-rich silicates as major bearing phases. PC3 groups concerned in situ As and Pb concentrations (11.7% of the total variance), and this was the PC with only TE. PC4 was associated with phosphates as only P concentrations were identified significantly. PC5 was linked to carbonates as there was a significant correlation with only Ca concentrations. PC6 was associated with the chalcophile group with sulfides and/or sulfates (positive correlation with only S concentrations).

When PCA was applied to station subgroups, the first four PCs (PC1 to 4) were relevant, explaining 62.3% of the total variance for the downstream station (Table 3b and Electronic Supplementary Material, SI 2) and 56.0% for the upstream station (Table 3c). At the downstream station, PCs defined the same main mineralogical groups as those of the whole dataset. However, TE correlations with major elements were more significant than with the whole dataset. PC1 was positively correlated with aluminosilicates and negatively with Cr-rich (Fe, Ti) oxides and heavy minerals. PC2 appeared to reflect Mn-rich particles with in situ Cu, Ni, and Zn correlations. PC3 was associated with phosphate, As, and Pb concentrations. PC4 appeared to represent carbonates (significant correlations with Ca and Mg) without any TE. At the upstream station, slight differences in major and trace element distributions could be noticed compared with the downstream station. PC1 was again positively associated with aluminosilicates and negatively with P-rich (Fe, Mn) oxides and with As, Pb, and Zn concentrations. The other PCs showed less clearly defined links between major and trace elements: PC2 positively included in situ P and Na concentrations and negatively Cr, Ni, and Pb concentrations; PC3 was positively associated with Ti concentrations and negatively with Ni and Zn, and PC4 was only moderately linked with in situ Mg concentrations.

Hence, according to the PCA performed, three main mineralogical groups were evidenced on both the whole dataset and on the subgroups of station locations: (i) aluminosilicates with K being the major associated cation, (ii) (Fe, Ti) oxyhydroxides and/or heavy minerals, (iii) Mn-rich particles. Phosphates, carbonates, and S-rich particles as sulfides and/or sulfates were also identified as a potential mineralogical group. However, due to the very low in situ concentrations of P, Ca, and S, these elements could not be considered as forming bearing phases in our study because, even though they can exist as very small grains (< 1 μm), they could not

Table 3 Principal component analysis for major and trace element in situ compositions of sediments (a) for both up- and downstream stations, (b) for the upstream station, and (c) for the downstream station

	F1	F2	F3	F4	F5	F6
(a) All the dataset (both stations), $n = 111$						
Si	*0.870*					
Al	*0.774*					
Fe	− 0.663	− 0.388				
Mn		*0.714*				
Ti		− 0.301		− 0.377		− 0.515
P			0.376	*0.616*		
S						*0.791*
Mg			− 0.327	− 0.367	0.507	
Ca					*0.809*	
Na	0.367			0.415		
K	0.675				− 0.407	
As			*0.877*			
Cr	− 0.397			− 0.495		
Cu	− 0.301	0.617				
Ni	− 0.317	*0.832*				
Pb			*0.876*			
Zn		*0.715*				
Eigenvalues	3.227	2.566	1.993	1.376	1.269	1.026
% explained variance	18.986	15.096	11.727	8.095	7.464	6.034
% cumulative variance	18.986	34.083	45.811	53.907	61.371	67.405
(b) At the downstream station, $n = 58$						
Si	*0.883*		− 0.359			
Al	*0.826*				0.301	
Fe	*− 0.822*			− 0.305		
Mn		*0.909*				
Ti	− 0.583				0.452	
P			0.621		− 0.394	
S					− 0.305	
Mg			− 0.408	0.678		
Ca				*0.765*	− 0.374	
Na	0.491					
K	0.644			− 0.394		
As			*0.817*		0.411	
Cr	− 0.544				0.380	
Cu		*0.751*				
Ni		*0.934*				
Pb			*0.898*			
Zn		*0.803*				
Eigenvalues	3.6	3.1	2.4	1.4	1.2	
% explained variance	21.0	18.4	14.4	8.5	7.1	
% cumulative variance	21.0	39.4	53.8	62.3	69.4	
(c) At the upstream station, $n = 53$						
Si	*0.777*					
Al	*0.761*		− 0.375			
Fe	− 0.599			0.447		
Mn	− 0.435		− 0.361		0.575	
Ti			0.564	−0.371	− 0.369	

Table 3 (continued)

	F1	F2	F3	F4	F5	F6
P	− 0.479	0.563	− 0.336			
S				− 0.473	0.367	
Mg	0.326	− 0.334		0.708		
Ca	− 0.357					
Na	− 0.299	0.649	− 0.419			
K	0.632		− 0.453			
As	− 0.529					
Cr		− 0.642			− 0.473	
Cu			− 0.402		− 0.419	
Ni		− 0.483	− 0.489			
Pb	− 0.459	− 0.564		− 0.477		
Zn	− 0.567	− 0.397	− 0.522			
Eigenvalues	3.6	2.3	1.9	1.6	1.3	
% explained variance	21.4	13.7	11.5	9.4	7.9	
% cumulative variance	21.4	35.1	46.5	56.0	63.9	

Figures in italics when significantly high when > 0.7, non-italicized font when moderately significant with $0.5 < r < 0.7$, and omitted when < 0.3 for clarity

be observed with the techniques used in this study. Maximum levels of these elements were quantified in (Fe, Ti)-rich aluminosilicates: P concentrations reached up to 6.1 %wt, Ca concentrations up to 14.0 %wt, and S concentrations up to 2.5 %wt. None of the grains analyzed could be considered representative of these mineralogical groups.

This first statistical step determined three main mineralogical groups: aluminosilicates, Fe and Ti oxyhydroxides, and Mn-rich particles. However, specific associations with representative quantified TE were not clearly determined, probably due to the wide range of TE-bearing phase chemistry. Hence, in situ chemical compositions required finer sorting in order to classify all the particles studied into these three TE-bearing groups. The following criteria were added:

i. Aluminosilicates were characterized with their in situ sum (Si+Al) higher than 20 %wt and up to 41.4 %wt (Table 2), and they represented 42 of the 111 significant EPMA analyses. K and Na represented the most and least concentrated cations, respectively (Table 2). Some of these silicate aggregates also occasionally included elements such as Ti and Fe, with levels up to 5.5 and 30.3 % wt, respectively. A subdivision was then identified in this group: aluminosilicates and (Fe, Ti)-rich aluminosilicates. The latter were distinguished from Fe oxyhydroxides and Ti-rich Fe oxyhydroxides according to their (Fe+Ti) sum (Fig. 2). The (Fe+Ti) sum of aluminosilicates and (Fe, Ti)-rich aluminosilicates was below 30 %wt, while, for Fe oxyhydroxides and Ti-rich Fe oxyhydroxides, it was higher than 40 %wt.

   The most concentrated TE quantified in this type of bearing phase were Zn, up to 3810 mg kg^{-1} in (Fe, Ti)-rich silicate aggregates (Table 2) and Pb (26,010 mg kg^{-1}) in aluminosilicates. Concentrations of Cr and Ni were low with a maximum of 1100 mg kg^{-1}. In general, As and Cu could not be quantified through EPMA (detection limit = 1000 mg kg^{-1}).

ii. The second significant PCA group was (Fe, Ti) oxyhydroxides, and during SEM sessions, they were the most frequently observed type of TE-bearing grains. All the particles assigned to this group had Fe as the most concentrated element, with concentrations ranging from 36.5 to 70.2 %wt. The Fe oxyhydroxides contained some minor elements such as Mn (up to 0.8%wt) and Ti (up to 0.6 %wt; Table 2). Mn-rich Fe oxyhydroxides had Mn concentrations ranging from 1.0 to 7.5% wt with a molar Mn/Fe ratio up to 0.3. (Ti, Fe) oxides showed Ti concentrations up to 14.8 %wt, Fe concentrations up to 62.9 %wt with a molar Ti/Fe ratio up to 0.3.

   All these (Fe, Ti) oxyhydroxides contained some of the studied TE, and in general, these TE showed maximum in situ concentrations in all the analyses performed. Detected Zn concentrations reached up to 1.69% in Fe oxyhydroxides and 2.29 %wt in Mn-rich Fe oxyhydroxides. In this type of particle, Pb was the second most concentrated TE. Its concentrations varied between 1950 mg kg^{-1} in Mn-rich Fe oxyhydroxides and 8180 mg kg^{-1} in (Ti, Fe) oxides. The other four TE detected (As, Cr, Cu, and Ni) were occasionally present in these oxyhydroxides. Arsenic was only present in Fe oxyhydroxides, with concentrations up to 2040 mg kg^{-1}. Copper was present in all the types of

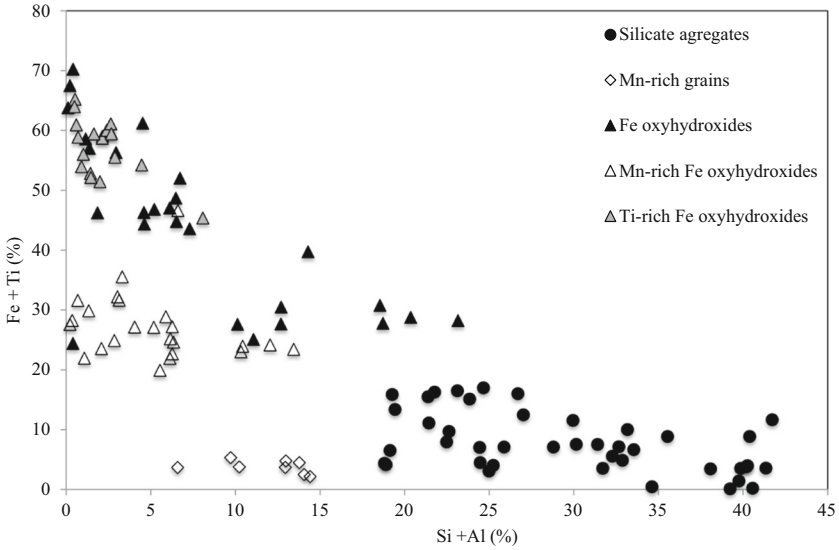

Fig. 2 In situ (Fe+Ti) concentrations versus in situ (Si+Al) concentrations (EPMA determined) in various TE-bearing phases of Loire sediments

(Fe, Ti) oxyhydroxides, and its concentrations varied from 1210 to 2000 mg kg^{-1}. Maximum concentrations of Cr and Ni were in (Ti, Fe) oxides (2060 mg kg^{-1}) and Fe oxyhydroxides (1650 mg kg^{-1}), respectively. No significant binary relationship could be determined between TE and Fe contents at the particle scale.

iii. Mn-rich grains were identified as the third PCA group. Manganese was mainly detected as a trace element during this study, at a level below 1.2% in aluminosilicates and (Fe, Ti)-rich silicate aggregates, Fe oxyhydroxides, and (Ti, Fe) oxides (Table 2). It was enriched up to 7.5 %wt in highly localized areas of Mn-rich Fe oxyhydroxides (Table 2). However, a few particles contained Mn as the major element, ranging from 21.1 to 31.9 %wt and these particles were classified as Mn oxyhydroxides. They did not occur frequently as only eight EPMA analyses corresponded to this class. Trace elements associated with these Mn oxyhydroxides such as Cu, Ni, Pb, and Zn were quantified, but no As or Cr was detected in this type of mineral. Maximum concentrations of Cu, Ni, and Pb were 2570 mg kg^{-1}, 7550 mg kg^{-1}, and 5190 mg kg^{-1}, respectively, and for Zn maxima ranged from 2590 to 16,910 mg kg^{-1}; one of the highest Zn concentrations was found with Mn-rich Fe oxyhydroxides (Table 2). Mn-rich particles showed the highest quantified TE concentrations among all the EPMA analyses.

3.2 Mineralogical characterization of TE-bearing phases

In addition to the in situ chemical composition, mineralogical characterization carried out using μSXRD and EPMA analyses did not enable two mineralogical species to be differentiated due to (i) EPMA-pear interactions and (ii) a same chemical composition corresponding to different crystal lattice organization. In this study, μSXRD analyses were carried out on the same zones which were studied by EPMA in order to provide combined chemical and mineralogical information. Mineralogical μSXRD maps were also very useful to define the mineralogy of aggregates in detail as this type of grain combination was very common in the sediments studied.

3.2.1 Mineralogy of aluminosilicates

As highlighted above (section 3.1), the first and main PC was associated with aluminosilicates for both the stations of the Loire river basin studied. When considering SEM images for all significant EPMA concentrations, these aluminosilicates were linked to fine-grained, highly divided aggregates (Figs. 3 and 4a). They appeared complex, very heterogeneous, and with multiphases. They were usually associated with low-contrast materials, attributed to a matrix of organic matter. At first glance, these organo-silicates represented a clay mix of illite-muscovite, phlogopite, chlorite, montmorillonite, and kaolinite compared with the in situ chemical composition of major elements composed of various clays described by Velde (1985). This clay assemblage is quite representative of the mineralogical composition of bulk sediments of the Loire river basin (Brossé 1979).

At a grain scale, some occasional Fe, Mn, and/or Ti enrichments could be noticed in these organo-silicated aggregates, linked to the presence of small grains of (Fe, Mn) oxyhydroxides and Ti oxides. For example, the EDS-SEM elemental map in Fig. 3 clearly shows clay sheets associated with the microscale distribution of Si, Al, and K and an enrichment of Fe and Mn located between the clay sheets. In the μSXRD-associated map (40 × 72 μm^2), kaolinite was

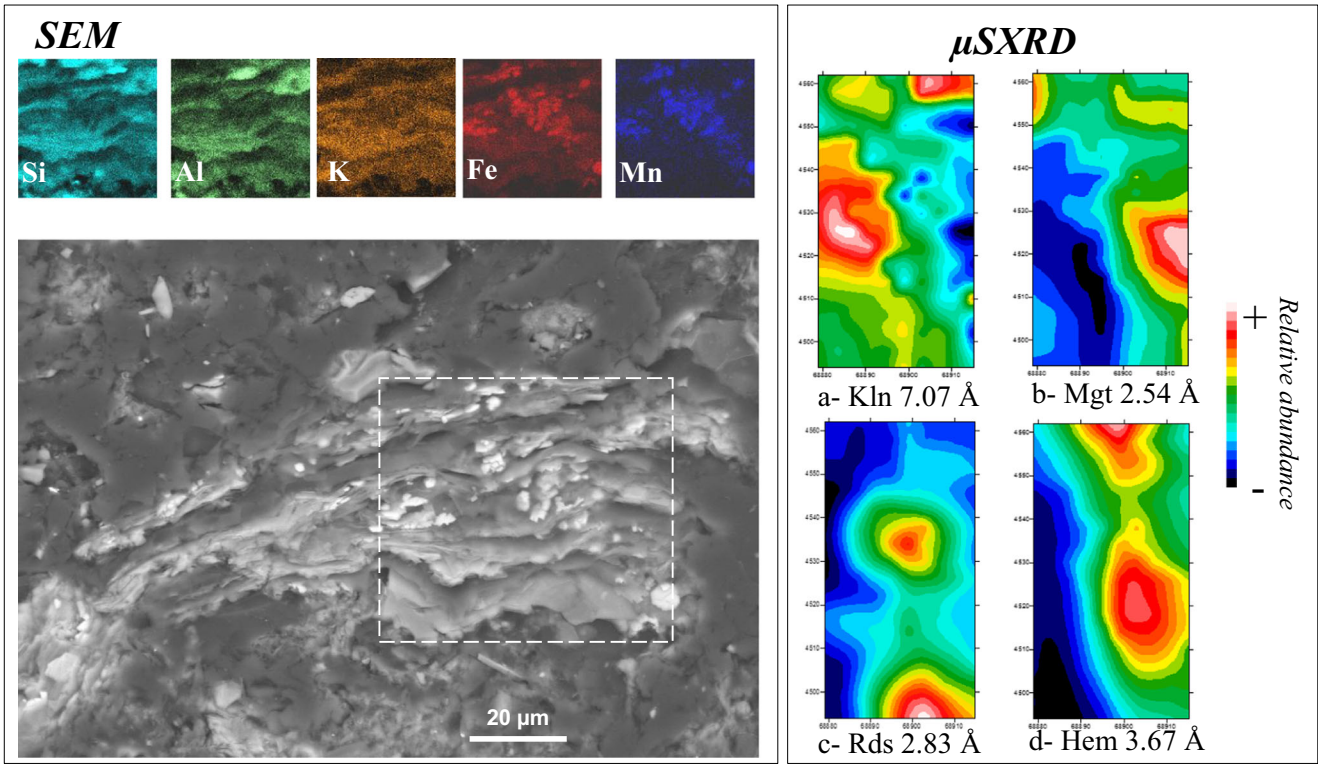

EPMA

in Fe oxyhydroxides		in silicates	in Fe oxyhydroxides	in silicates
Si (%)	1.8-7.5	9.2-18.4	As (ppm)	-	-
Al (%)	1.2 – 5.9	6.4-7.4	Cu (ppm)	up to 1200	-
Fe (%)	22.2-35.2	2.3-10.6	Pb (ppm)	up to 1300	-
Mn (%)	3.2-7.5	0.1-4.4	Zn (ppm)	up to 2400	up to 2300

Fig. 3 In situ characterization of a silicate aggregate (BSE-SEM image) in Loire sediments showing the distribution of magnetite/hematite and rhodocrosite grains associated with (Fe, Mn) enrichment EDS-SEM and (Mgt, Rds, and Hem) µSXRD maps (40 × 72 µm^2). These grains were embedded in clay sheets, mostly kaolinite associated with (Si, Al, K) enrichment EDS-SEM and Kln µSXRD maps (40 × 72 µm^2). Minimum and maximum concentrations determined by EPMA are given for both types of grain. Mineral abbreviations for µSXRD maps are a- Kln, kaolinite; b- Mgt, magnetite Fe_3O_4; c- Rds, rhodochrosite $MnCO_3$; d- Hem, hematite Fe_2O_3

identified and represented clearly distinct clay sheets. The magnetite and hematite signals corresponded to the well-marked micrograins and associated with the Fe-enrichment. These Fe-oxides also showed some local Mn-enrichment. A rhodocrosite µXRD signal was detected and could be linked to this local Mn-enrichment.

Some trace elements were EPMA quantified in these selected organo-silicate aggregates. The presence of As, Cr, Cu, Ni, Pb, and Zn was detected, but their respective in situ concentrations were usually below quantification limits except for Zn, whose concentration was often above quantification limits.

Relationships between various major elements and in situ Zn concentrations were tested in order to identify which fine-grained minerals could represent Zn-bearing phases. Regarding in situ concentrations among all the organo-silicate aggregates mentioned in the previous paragraph (21 aggregates, 42 in situ analyses including 26 Zn in situ concentrations above the QL), Zn was more significantly correlated with Fe and P ($r^2 = 0.277$ and $r^2 = 0.401$, respectively) than with (Si+Al) ($r^2 < 0.1$; Electronic Supplementary Material, SI 2). However, this seems to depend on the aggregate at this grain scale. In Fig. 3, in situ Zn concentrations, ranging from 1200 to 2400 mg kg^{-1}, appear to be more closely related to the in situ concentrations of (Si+Al) and P ($r^2 = 0.236$, $r^2 = 0.190$; 16 analyses with Zn > QL) than to those of Fe or Mn ($r^2 < 0.15$). Zinc-bearing phases would be P-rich clays rather than magnetite/hematite in this particular case.

3.2.2 Mineralogy of Fe oxyhydroxides

Based on in situ chemical characterization, Fe oxyhydroxides were the easiest TE-bearing phases to visualize as their SEM

detection was related to a very characteristic chemical composition, iron being the major element detected. They contained between 36.5 and 70.2 %wt in situ Fe concentrations (Table 2). In addition, some of these Fe oxyhydroxides contained minor elements of Ti and Mn (Table 2).

In this study, Fe oxyhydroxides present in Loire river bed sediments occurred in other particles (Figs. 3 and 4a, b), as silicate coatings (Fig. 4c) or as isolated grains (Fig. 4d). They varied from quite small (< 10 μm) to large particles (> 50 μm), depending on their habitus. When isolated, they were relatively large grains, at least 10 μm in their longest axis and they were more or less weathered (Fig. 4d). These were mostly identified as goethite or hematite through μSXRD. Even if ferrihydrite is one of the most ubiquitous and frequent Fe(III) oxyhydroxides in sediments (Jambor and Dutrizac 1998; Cismasu et al. 2011), no ferrihydrite or amorphous Fe oxides were detected by μSXRD in the selected Fe-rich particles studied here and if present, they may only have been nano-particles. The Fe oxyhydroxides observed as isolated grains were included within other grains or aggregates (Figs. 3 and 4a, b). In this case, Fe-oxyhydroxide grains were smaller (< 10 μm), identified as goethite, magnetite, and/or hematite depending on the sample. A few Fe-hydroxide coatings were also clearly observed (Fig. 4c): Goethite was always determined as the coating mineral in the few μSXRD analyses performed.

These oxyhydroxides contained trace elements such as As (up to 2040 mg kg^{-1}), Cr (up to 1300 mg kg^{-1}), Cu (up to 2000 mg kg^{-1}), and Ni (up to 1650 mg kg^{-1}; Table 2). The most concentrated TE in this type of mineral were Pb and Zn (up to 2540 mg kg^{-1} and 16,910 mg kg^{-1}, respectively). However, at a particle scale, no significant Fe-TE relationship could be determined despite the large number of EPMA analyses for these types of bearing phases (61 analyses in total)

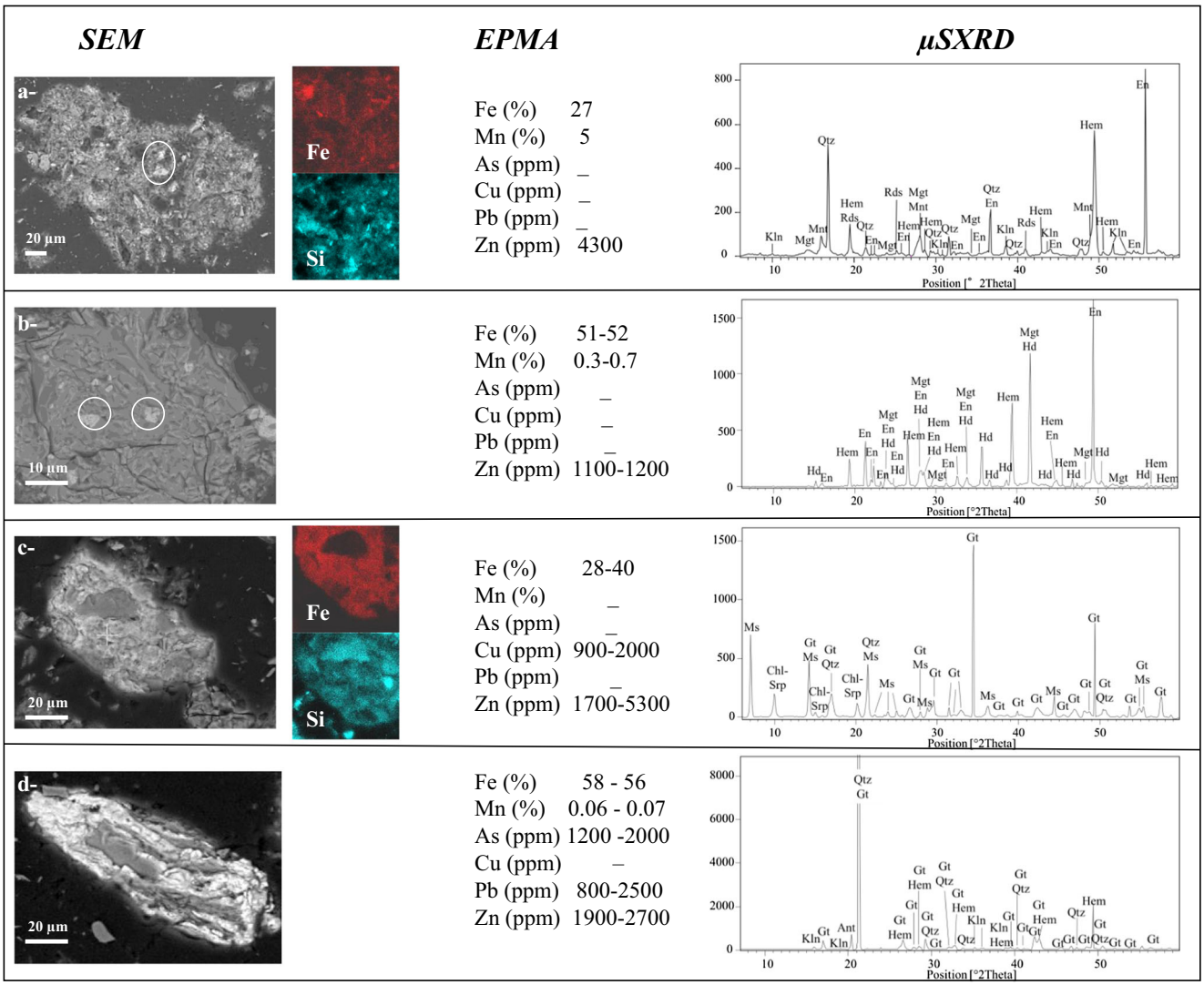

Fig. 4 In situ characterization of various representative oxyhydroxides observed in Loire sediments (BSE-SEM image, EDS-SEM elemental map, EPMA concentrations, and μSXRD mineralogical identification). Mineral abbreviations for μSXRD patterns are Ant, anatase; Chl-Srp, chlorite-serpentinite; En, enstatite; Gt, goethite; Hd, hedenbergite; Hem, hematite; Kln, kaolinite; Mgt, magnetite; Mnt, montmorillonite; Ms, muscovite; Rds, rhodocrosite; Qtz, quartz. Scale bar for SEM image

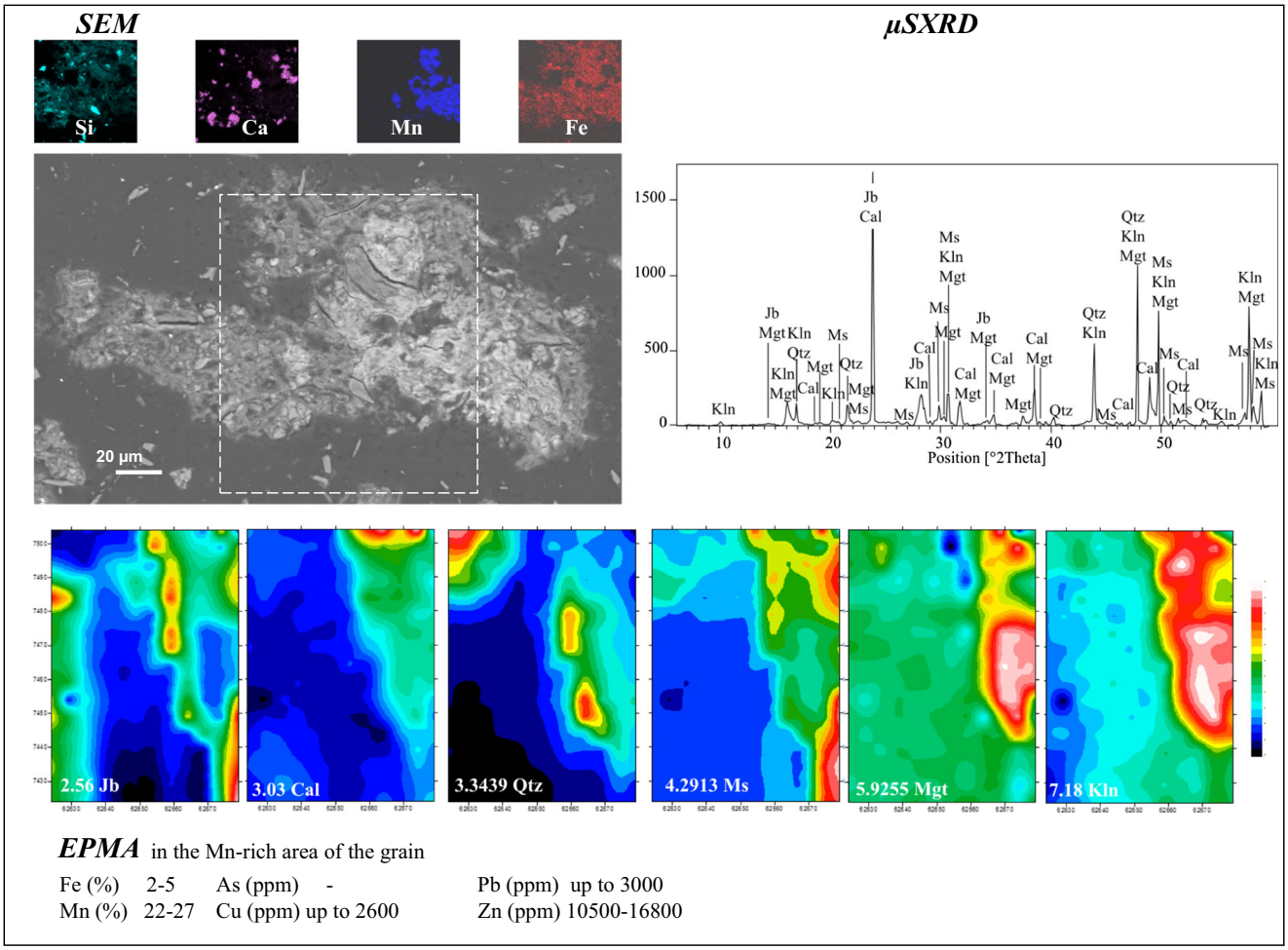

Fig. 5 In situ characterization of a Mn-rich grain observed in Loire sediments (BSE-SEM image, EDS-SEM elemental map, EPMA concentrations), associated with jacobsite (µSXRD identification with diffractogram and map). Mineral abbreviations for µSXRD are Cal, calcite; Jb, jacobsite; Kln, kaolinite; Mgt, magnetite; Ms, muscovite; Qtz, quartz. Scale bar for SEM image

and no link between oxyhydroxide mineralogy and in situ TE concentrations could be found either.

3.2.3 Mineralogy of Mn-rich grains

Manganese was detected mainly as a trace element in various types of TE-bearing phases (< 1.2 %wt) and also enriched in the so-called Mn-rich Fe oxyhydroxides (Table 2). When Mn concentrations ranged from 21.2 to 31.9 %wt, these minerals were clearly Mn-rich particles. However, they were rarely found in the Loire sediments studied here. Only two Mn-rich particles were detected by µSXRD and corresponded to eight validated EPMA analyses. Using µSXRD, one was identified as jacobsite ($MnFe_2O_4$) and contained between 26 and 32 wt% Mn (Fig. 5) and the other was a Mn-silicate belonging to the braunite group ($Mn^{2+}Mn^{3+}{}_6SiO_{12}$). Although these minerals were not representative of Mn-rich grains due to their very low occurrence among all the in situ observations, they were unusual enough to be mentioned here as they contributed greatly to the bulk Mn concentrations in a sediment sample. In addition, these Mn-rich minerals were among the most TE-concentrated phases, especially in Zn (2.3 %wt Zn in Mn-rich Fe oxyhydroxides, Table 2) and they also actively contributed to the bulk TE concentrations in sediments.

4 Conclusions

This approach which combines several microscale techniques is a relatively common methodology to assess the environmental impacts of mining ore and waste alteration (i.e., Courtin-Nomade et al. 2005, 2010; Moberly et al. 2009; Kierczak et al. 2013). In the present study, it was interesting to adapt it to identify TE-bearing phases and their state in sediments and to quantify in situ concentrations in grains by combining both chemical and mineralogical analyses. Three main mineralogical groups were evidenced through PCA performed on in situ concentrations and fine sorting classification based on in situ concentrations and µSXRD data. Fine-

grained aggregates of aluminosilicates were frequently detected, consisting of multiphases associated with an organic matrix. They were mostly Zn and Pb enriched (up to 3810 and 2610 mg kg^{-1}, respectively), with Cr and Ni levels lower than 1100 mg kg^{-1}, but no As or Cu. Through SEM, Fe oxyhydroxides enriched with Mn and Ti were predominantly observed as isolated grains or silicate coatings, or included in aggregates. They presented the highest in situ concentrations detected in all the TE studied. In contrast, Mn-rich particles were statistically significant as a mineralogical group but were not very frequently observed. When present, they contribute greatly in concentrating TE and especially Zn. All these characterized non-organic TE-bearing phases are quite common, non-site specific and can be considered representative of a commonly studied river basin as already described (Grosbois et al. 2007; Courtin-Nomade et al. 2009, 2016). Phosphates, carbonates, and S-rich particles such as sulfides and/or sulfates were also identified as a potential mineralogical group using PCA but could not be considered representative of a major TE-bearing group because of the very low in situ concentrations of P, Ca, and S.

The approach presented in this study demonstrates both advantages and limitations. It gives an overview of the major TE-bearing phases, providing simultaneously both elemental and mineralogical information about the same particle or aggregate. It is non-destructive and reveals a much more complex mineralogy and particle association of TE-bearing phases than could ever be obtained through operationally defined procedures. Isolated particles, multiple grain aggregates and coatings were evidenced showing how heterogeneous they can be at a microscale. However, this analytical procedure has some limitations: (i) it has to be used randomly and with accuracy to be truly representative, and this is time-consuming; (ii) it does not consider organic matter as a major TE-bearing phase, another main component of sediments, which reacts readily with trace elements. This type of association is therefore under-estimated. Besides, SEM and EPMA techniques mainly provide information about the nature of bearing particles but they do not give direct information about the type of bonding between TE and bearing phases. This approach has been completed with μSRXD, and additional in situ techniques including transmitted electron microscopy (TEM), X-ray fluorescence mapping, or X-ray absorption spectroscopy such as EXAFS could also be investigated; (iii) the ratio between the EPMA/μSXRD beam size and the particle analyzed is a very important parameter to take into account. Bearing phases, presenting just a few microns, could not be studied, nor could nano-Fe oxides and highly divided particles in organo-silicate aggregates, and (iv) it is important to quantify the representativeness of the main mineralogical groups. Previous studies have used calibrated SEM equipped with an automated particle counting and classification system (Franke et al. 2009; Grosbois et al. 2011; Marchandise et al. 2014). Grosbois et al. (2011) showed good correspondence for frequency determination between the method using calibrated SEM (automation using about 1000 individual analyzed particles) and the methodology presented in this study.

This in situ and non-destructive approach is accurate at determining the precise microscale distribution of trace elements. It represents the first step in assessing long-term contamination risk throughout trace element cycles. Determining the potential mobility of TE during the sediment cascade and post-depositional processes in sediment reservoirs can be investigated further when these results are combined with other approaches such as TEM and spectroscopic methods.

Acknowledgments The authors greatly appreciated the high quality of analyses and discussions with the IBiSA platform of the University of Tours regarding SEM analyses (microscopies.med.univ-tours.fr) and with the MEN/CAMPARIS platform for EPMA analyses (UPMC, IPGP, UDD, MNHN, ENS, CSNSM, IN2P3, University of Poitiers and of La Rochelle; camparis.ecceterra.fr). X-ray diffraction was carried at the UMR 7347 GREMAN lab (University of Tours). MicroSXRD were performed at the Advanced Light Source at Lawrence Berkeley National Laboratory (CA, USA). The microdiffraction program at the ALS on beamline 12.3.2 was made possible by NSF grants in 2012 and 2014. The authors also like to thank Susan Edrich (Interconnect LC) for her re-reading of this manuscript.

Funding information The financial support for this long research program was multiple, and authors would like to thank the French organizations which fund research on the Loire basin (Agence de l'Eau Loire-Bretagne, Etablissement Public Loire, the University of Tours and Limoges, France). This study was also partly funded by the European program FEDER run by the Conseil Regional Centre-Val de Loire, referenced as 2016-110381.

References

Audry S, Schafer J, Blanc G, Jouanneau J (2004) Fifty-year sedimentary record of heavy metal pollution (Cd, Zn, Cu, Pb) n the Lot river reservoirs (France). Environ Pollut 132:413–426

Bednarova Z, Kuta J, Kohut L, Machat J, Klanova J, Holoubek I, Jarkovnsky J, Dusek L, Hilscherova K (2013) Spatial patterns and temporal changes of heavy metal distributions in river sediments in a region with multiple pollution sources. J Soils Sediments 13(7): 1257–1269

Blute NK, Jay JA, Swart CH, Brabander DJ, Hemond HF (2009) Aqueous and solid phase arsenic speciation in the sediments of a contaminated wetland and riverbed. Appl Geochem 24:346–358

Bonner FW, Bridges JW (2016) Toxicological properties of trace elements. In: Rose J (ed) Trace elements in health: a review of current issues. Butterworths, Cambridge, pp 1–20

Bureau des recherches géologiques et minières (2017) Nouvelle carte géologique de la France à 1/1000000. 6ème édition

Brossé R (1979) La sedimentation argileuse et chimique de la Loire dans son cours moyen, de Gien à Tours. Norois 101:90–100

Brossé R (1982) Les processus sédimentaires dans le fleuve Loire. Dissertation, University of Angers, France

Byrne P, Taylor KG, Hudson-Edwards KA, Barrett JES (2017) Speciation and potential long-term behavior of chromium in urban sediment particulates. J Soils Sediments 17:2666–2676

Carroué JP (2010) Les richesses minerals de la Loire. Géosciences 12: 100–112

Charlet L, Manceau A (1993) Structure, formation and reactivity of hydrous oxide particles: insights from x-ray absorption spectroscopy. In: Buffle J, van Leeuwen HP (eds) Environmental Particles. Lewis Publishers, pp 117–164

Ciffroy P, Garnier JM, Benyahya L (2003) Kinetic partitioning of Co, Mn, Cs, Fe, Ag, Zn and Cd in fresh waters (Loire) mixed with brackish waters (Loire estuary): experimental and modelling approaches. Mar Pollut Bull 46:626–641

Cismasu AC, Michel FM, Tcaciuc AP, Tyliszczak T, Brown GE Jr (2011) Composition and structural aspects of naturally occurring ferrihydrite. Compt Rendus Geosci 343:210–218

Costa-Miguens F, Lima de Oliviera M, de Oliviera Ferreira A, Rodrigues Barbosa L, Tenorio de Melo J, Veiga de Carvalho CE (2016) Structural and elemental analysis of bottom sediments from the Paraiba do Sul river (SE Brazil) by analytical microscopy. J S Am Earth Sci 66:82–96

Courtin-Nomade A, Grosbois C, Bril H, Roussel C (2005) Spatial variability of arsenic in some iron-rich deposits generated by acid-mine drainage. Appl Geochem 20:383–396

Courtin-Nomade A, Grosbois C, Marcus MA, Fakra SC (2009) The weathering of a sulfide orebody : speciation and fate of some potential contaminants. Can Min 47(3):493–508

Courtin-Nomade A, Bril H, Bény JM, Kunz M, Tamura N (2010) Sulfide oxidation observed using micro-Raman spectroscopy and micro-X-ray diffraction: the importance of water/rock ratios and pH conditions. Am Mineral 95:582–591

Courtin-Nomade A, Waltzing T, Evrard C, Soubrand M, Ducloux E, Ghorbel S, Grosbois C, Bril H (2016) Arsenic and lead mobility : from tailing materials to the aqueous compartment. Appl Geochem 64:10–21

Dhivert E, Grosbois C, Coynel A, Lefevre I, Desmet M (2015) Influences of major flood sediment inputs on sedimentary and geochemical signals archived in a reservoir core (Upper Loire basin France). Catena 126:75–85

Dhivert E, Grosbois C, Courtin-Nomade A, Bourrain X, Desmet M (2016) Dynamics of metallic contaminants at a basin scale – spatial and temporal reconstruction from four sediment cores (Loire fluvial system, France). Sci Total Environ 541:1504–1515

Drahota P, Rohovec J, Filippi M, Mihaljevic M, Rychlovsky P, Cerveny V, Pertold Z (2009) Mineralogical and geochemical controls of arsenic speciation and mobility under different redox conditions in soil, sediment and water at the Mokrsko-west gold deposit, Czech Republic. Sci Total Environ 407:3372–3384

Du Laing G, Rinklebe J, Vandecasteele E, Meers E, Tack FMG (2009) Trace metal behavior in estuarine and riverine floodplain soils and sediments: a review. Sci Total Environ 407:3972–3985

Dudka S, Adriano DC (1997) Environmental impacts of metal ore mining and processing: a review. J Environ Qual 26:590–602

Favas PJC, Patras J, Gomes EP, Cala V (2011) Selective chemical extraction of heavy metals in tailings and soils contaminated by mining activity: environmental implications. J Geochem Explor 111:160–171

Fialin M, Remy H, Richard C, Wagner C (1999) Trace element analysis with the electron microprobe : new data and perspectives. Am Min 84:70–77

Forstner U, Salomons W (2008) Trace elements and compounds in sediments. In: Elements and their compounds in the environment: occurrence, analysis and biological relevance. Merian E, Anke M, Ihnat M, Stoepler M ed. Wiley-VCH, 1806:149–162

Forstner U, Heise S, Schwartz R, Westrich B, Ahlf W (2004) Historical contaminated sediments and soils at the river basin scale. Examples from the Elve river catchment area. J Soils Sediments 4:247–260

Franke C, Kissel C, Robin E, Bonte P, Lagroix F (2009) Magnetic particle characterization in the Seine river system : implications for the determination of natural versus anthropogenic. Input. Geochem Geophys Geosyst 10(8):1–20

Frau F, Ardau C, Fanfani L (2009) Environmental geochemistry and mineralogy of lead at the old mine area of Baccu Locci (south-east Sardinia, Italy). J Geochem Explor 100:105–115

Garban B, Ollivon D, Carru AM, Chesterikoff A (1996) Origin, retention and release of trace metals from sediments of the river Seine. Water Air Soil Poll 87:363–381

Garcia-Lorenzo M, Perez-Sirvent C, Molina-Ruiz J, Martinez-Sanchez MJ (2014) Mobility indices for the assessment of metal contamination in soils affected by old mining activities. J Geochem Explor 147:117–129

Gleyzes C, Tellier S, Astruc M (2002) Fractionation studies of trace elements in contaminated soils and sediments: a review of sequential extraction procedures. Tr Analyt Chem 21(6–7):451–467

Grosbois C, Negrel P, Grimaud D, Fouillac C (2001) An overview of dissolved and suspended matter fluxes in the Loire river basin: natural and anthropogenic inputs. Aquat Geochem 7(2):81–105

Grosbois C, Courtin-Nomade A, Martin F, Bril H (2007) Transportation and evolution of trace element bearing phases in stream sediments in a mining-influenced basin (upper isle river, France). Appl Geochem 22:2362–2374

Grosbois C, Courtin-Nomade A, Robin E, Bril H, Tamura N, Schafer J, Blanc J (2011) Fate of arsenic-bearing phases during the suspended transport in a gold mining district (Isle river basin, France). Sci Total Environ 409(23):4986–4999

Grosbois C, Meybeck M, Lestel L, Lefevre I, Moatar F (2012) Severe and contrasted polymetallic contamination patterns (1900-2009) in the Loire river sediments (France). Sci Total Environ 435-436:290–305

Horowitz AJ, Elrick KA (1987) The relation of stream sediment surface area, grain size and composition to trace element chemistry. Appl Geochem 2(4):437–451

Horowitz AJ, Stephen VC (2008) The effects of land use on fluvial sediment chemistry for the conterminous U.S.- results from the first cycle of the NAWQA program: trace and major elements, phosphorus, carbon and sulfur. Sci Total Environ 400(1–3):290–314

Hudson-Edwards KA, Houghton SL, Osborn A (2004) Extraction and analysis of arsenic in soils and sediments. Tr Analyt Chem 23(10–11):745–752

Jack CN, Juhasz A, Smith E, Naidu R (2015) Assessing the bioavailability and bioaccessibility of metals and metalloids. Environ Sci Pollut Res 22:8802–8825

Jambor JL, Dutrizac JE (1998) Occurrence and constitution of natural and synthetic ferrihydrite, a widespread iron oxyhydroxide. Chem Rev 98:2549–2586

Kabata-Pendias A, Sadurski W (2008) Trace elements and compounds in soils. In: Merian E, Anke M, Ihnat M, Stoepler M (ed) Elements and their compounds in the environment: occurrence, analysis and biological relevance. Wiley-VCH, 1806:79–99

Kierczak J, Potysz A, Pietranik A, Tyszka R, Modelska M, Neel C, Ettler V, Mihaljevic M (2013) Environmental impact of the historical Cu smelting in the Rudawy Janowickie mountains (South-western Poland). J Geochem Explor 124:183–194

Kunz M, Tamura N, Kai Chen K, MacDowell AA, Celestre RS, Church MM, Fakra S, Domming EE, Glossinger JM, Kirschman JL, Morrison GY, Plate DW, Smith BV, Warwick T, Yashchuk VV, Padmore HA, Ustundag E (2009) A dedicated superbend X-ray microdiffraction beamline for materials, geo- and environmental sciences at the advanced light source. Rev Sci Instrum 80:35–108

Larrose A, Coynel A, Schafer J, Blanc G, Masse L, Maneux E (2010) Assessing the current state of the Gironde estuary by mapping priority contaminant distribution and risk potential in surface sediments. Appl Geochem 25(12):1912–1923

Le Cloarec MF, Bonté P, Lestel L, Lefevre I, Ayrault S (2009) Sedimentary record of metal contamination in the Seine river during the last century. Phys Chem Earth 36(12):515–529

Le Gall M, Evrard O, Foucher A, Laceby JP, Salvador-Blanes S, Manière L, Lefèvre I, Cerdan O, Ayrault S (2017) Investigating the temporal dynamics of suspended sediment during flood events with 7Be and 210Pbxs measurements in a drained lowland catchment. Sci Rep. https://doi.org/10.1038/srep42099

Macaire JJ, Gay-Ovejero I, Bacchi M, Cocirta C, Patryl L, Rodrigues S (2013) Petrography of alluvial sands as a past and present environmental indicator : case of the Loire river (France). Int J Sediment Res 28:285–303

Manickam S, Barbaroux L, Ottman F (1985) Composition and mineralogy of suspended sediments in the fluvio-estuarine zone of the Loire river (France). Sedimentology 32:721–741

Marchandise S, Robin E, Ayrault S, Roy-Barman M (2014) U-Th-REE-Hf bearing phases in Mediterranean Sea sediments: implications for isotope systematics in the ocean. Geochim Cosmochim Ac 131:47–61

Miler M, Gosar M (2015) Chemical and morphological characterictics of solid metal-bearing phases deposited in snow and stream sediments as indicators of their origin. Environ Sci Pollut R 22(3):1906–1918

Moberly JG, Borch T, Rajesh KS, Spycher NF, Sevinc-Sengor S, Ginn TR, Pyeton BM (2009) Heavy metal-mineral associations in Coeur d'Alene river sediments: a synchrotron-based analysis. Water Air Soil Poll 201:195 208

Montarges-Pelletier E, Duriez C, Ghanbaja J, Jeanneau L, Falkenberg G, Michot LJ (2014) Microscale investigations of the fate of heavy metals associated to iron-bearing particles in a highly polluted stream. Environ Sci Pollut Res 21(4):2744–2760

Négrel P (1997) Multi-element chemistry of Loire estuary sediments: anthropogenic vs natural sources. Estuar Coast Shelf S 44:395–410

Novakova T, Grygar TM, Babek O, Famera M, Mihalievic M, Strnad L (2013) Distinguish regional and local sources of pollution by trace metals and magnetic particles in fluvial sediments of the Morava river, Czech Republic. J Soils Sediments 13(2):460–473

Nriagu JO, Skaar EP (2015) Trace metals and infectious diseases. MIT press, p 480

Potsma D, Jessen S, Thi MinhHue N, Thanh Duc M, Bender Koch C, Hung Viet P, Quy Nhan P, Larsen F (2010) Mobilization of arsenic and iron from red river floodplain sediments, Vietnam. Geochim Cosmochim Ac 74:3367–3381

Ryan PC, Hillier S, Wall AJ (2008) Spetwise effects of the BCR sequential chemical extraction procedure on dissolution and metal release from common ferromagnesian clay minerals: a combined solution chemistry and X-ray powder diffraction study. Sci Total Environ 407:603–614

Sparks DL (2005) Toxic metals in the environment: the role of surface. Elements 1:193–197

Tamura N, Padmore HA, Patel JR (2005) High spatial resolution stress measurements using synchrotron based scanning X-ray microdiffraction with white or monochromatic beam. Mater Sci Eng R 399:92–98

Velde B (1985) Clay minerals : a physico-chemical explanation of their occurrence. Elsevier, Amsterdam

Villanueva U, Raposo JC, Madariaga JM (2013) A new methodological approach to assess the mobility of As, Cd, Co, Cr, Cu, Fe, Ni and Pb in river sediments. Microchem J 106:107–120

Zhou G, Sun B, Zeng D, Wei H, Liu Z, Zhang B (2014) Vertical distribution of trace elements in the sediment cores from major rivers in East China and its implication on geochemical background and anthropogenic effects. J Geochem Explor 139:53–67